New Triphenylamine-Based Organic Dyes for Efficient Dye-Sensitized Solar Cells

Mao Liang,[†] Wei Xu,[†] Fengshi Cai,[†] Peiquan Chen,[‡] Bo Peng,[†] Jun Chen,*[,†] and Zhengming Li[‡]

Institute of New Energy Material Chemistry and Institute of Elemento-Organic Chemistry and State Key Laboratory of Elemento-Organic Chemistry, Nankai University, Tianjin 300071, People's Republic of China

Received: November 29, 2006; In Final Form: January 12, 2007

We report here on the synthesis and photophysical/electrochemical properties of a series of novel triphenylamine (TPA)-based organic dyes (TPAR1, TPAR2, TPAR4, and TPAR5) as well as their application in dye-sensitized nanocrystalline TiO_2 solar cells (DSCs). In the four designed dyes, the TPA group and the rhodanine-3-acetic acid take the role of the basic electron donor unit and the electron acceptor, respectively. It was found that introduction of a CH_2═CH− group into the TPA unit exhibited better photovoltaic performance due to the increase of the electron-density donor moiety and that introduction of a methine (−CH═CH−) unit to the π bridge resulted in a red-shift and broadening of the absorption spectrum due to expansion of the π-conjugation system. Density functional theory (DFT) calculation indicated that the electron distribution moved from the donor unit to the electron acceptor under light irradiation, which means efficient intramolecular charge transfer. In particular, the DSCs based on TPAR4 showed the best photovoltaic performance: a maximum monochromatic incident photon-to-current conversion efficiency (IPCE) of 81%, a short-circuit photocurrent density (J_{sc}) of 18.2 mA cm^{-2}, an open-circuit photovoltage (V_{oc}) of 563 mV, and a fill factor (ff) of 0.61, corresponding to an overall conversion efficiency of 5.84% under AM 1.5 irradiation (100 mW cm^{-2}). This work suggests that the molecular-designed triphenylamine dyes are promising in the application of DSCs.

Introduction

Dye-sensitized solar cells (DSCs) have received considerable attention for transferring clean solar energy into electricity over the past decade.[1] The inorganic−organic hybird DSCs have seen further scientific and industrial research, including the areas of designing more efficient dyes/sensitizers and electron mediators,[2] fabricating better nanostructured films,[3] replacing the cathode materials,[4] and more deeply understanding the interfacial charge-transfer process.[5] In the DSCs system, light is absorbed by the dye anchored on the TiO_2 surface and then electrons from the excited dye inject into the conduction band (CB) of the TiO_2, generating electric current, while the ground state of the dye is regenerated by the electrolyte to give efficient charge separation. It is thus that the dye in DSCs is essential for efficient light harvesting and electron generation/transfer.

Up to now, there have been two kinds of dyes, namely metal−organic complexes and metal−free organic dyes, which have been widely investigated as sensitizers of DSCs. The noble-metal ruthenium polypyridyl complexes such as N3 and black dye developed by Grätzel and co-workers[6−8] have proved to be the best dyes with overall energy conversion efficiency (η) greater than 10% under AM 1.5 irradiation. On the other hand, metal-free organic dyes have also been developed for DSCs owing to their high molar absorption coefficient, simple synthesis procedure, and structure variety. Recently, a number of metal-free organic dyes such as merocyanine,[9] hemicyanine,[10] cyanine,[11] coumarin,[12] perylene,[13] indoline,[14] oligothiophene,[15] dialkylaniline dyes,[16] and triphenylamine dyes[17] have been reported, which make the organic dyes fruitful in the application of DSCs. Among various metal-free organic dyes, indoline dye (D149),[14b] coumarin (NKX-2677),[12b] and oligothiophene dye (MK-2)[15a] exhibit a high η of 9.0%, 7.7%, and 7.7%, respectively.

In this paper, we report on the synthesis and characterization of four novel triphenylamine (TPA)-based dyes (Scheme 1) and their further application as sensitizers in DSCs. In our design, TPAR1 is the basic model, in which the TPA unit was connected to the rhodanine-3-acetic acid by one double bond. A methine unit was introduced to the π-conjugation bridge of TPAR1, resulting in TPAR2 that has a larger conjugation system than that of TPAR1. To enhance the electron-donor ability of TPA, an alkene was attached to the adjacent phenyl ring of TPAR1, leading to the structure of TPAR4. Either an alkene attachment to the adjacent phenyl ring of TPAR2 or a methine unit introduction to the π-conjugation bridge of TPAR4 can produce TPAR5. The combination of experimental study and density functional theory (DFT) calculation shows that the introduction of rich-electron groups to the adjacent phenyl ring of TPA-based dyes has a significant influence on the photovoltaic performance of the DSCs. It was found that a cell with TPAR4 as the dye exhibits a high overall energy conversion efficiency of 5.84%, indicating its potential application as the metal-free organic dyes in DSCs.

Experimental Section

Synthesis and Characterization. The starting materials 4-formaltriphenylamine (**1**), *N*-phenyl-*N*-(vinylphenyl)benzenamine (**2**), 4-(*N*-phenyl-*N*-(4-vinylphenyl)amino)benzaldehyde (**4**), and *N*-phenyl-4-vinyl-*N*-(4vinylphenyl)benzenamine (**5**) were prepared by adopting literature procedures.[18] All other solvents and chemicals used in this work were analytical grade

* Address correspondence to this author. E-mail: chenabc@nankai.edu.cn.

[†] Institute of New Energy Material Chemistry.

[‡] Institute of Elemento-Organic Chemistry and State Key Laboratory of Elemento-Organic Chemistry.

10.1021/jp067930a CCC: $37.00
Published on Web 03/01/2007

SCHEME 1: Molecular Structures of Triphenylamine Dyes

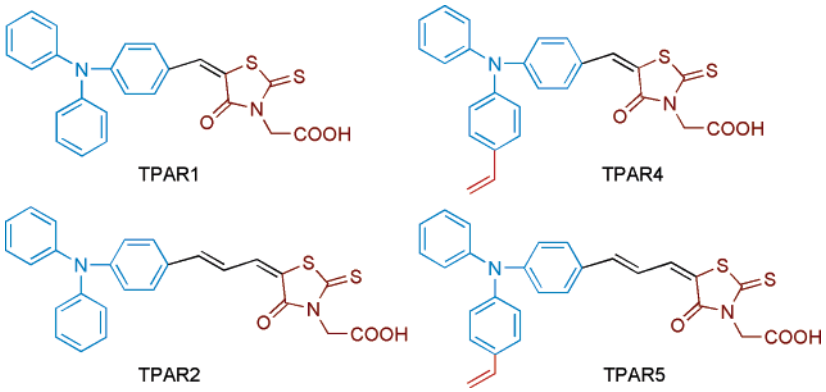

SCHEME 2: Synthetic Pathway of the Triphenylamine-Based Dyes (TPAR1, TPAR 2, TPAR 4, and TPAR 5)

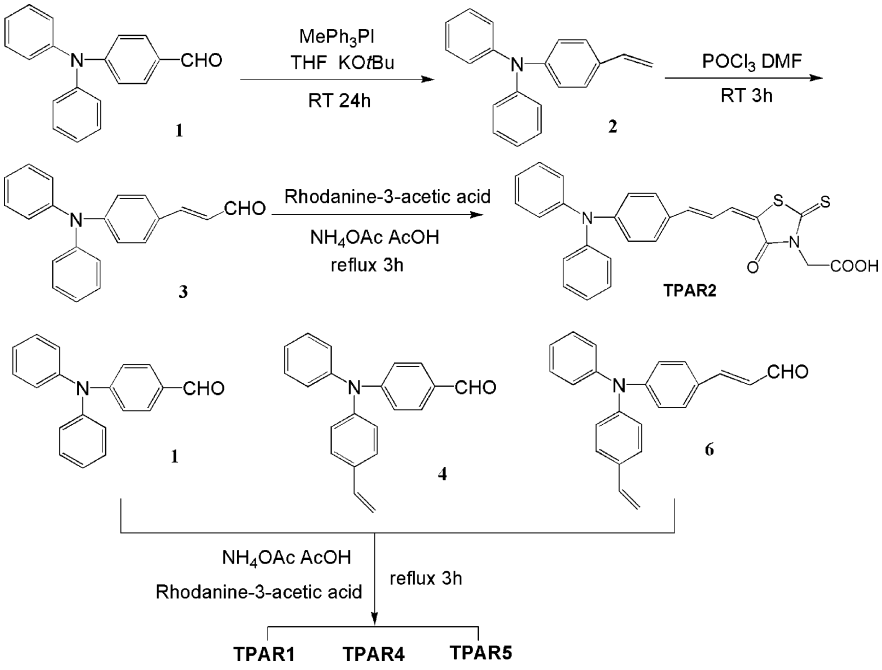

and were used without further purification. Potassium *tert*-butylate, tetrabutylammonium perchlorate, chenodeoxycholic acid (DCA), Triton X-100, 4-*tert*-butylpyridine (TBP), and 1,2-dimethylimidazole were pursed from Aldrich. N3 was synthesized according to the literature.[6] The synthetic pathway of the four dyes is shown in Scheme 2.

TPAR1: To 15 mL of glacial acetic acid were added 150 mg (0.55 mmol) of **1** and 110 mg (0.57 mmol) of rhodanine-3-acetic acid and the solution was refluxed for 3 h in the presence of 100 mg of ammonium acetate. After cooling to room temperature, the mixture was poured into ice water. The precipitate was filtered and washed with distilled water. After drying under vacuum, the precipitate was purified by recrystallization from ethanol, resulting in red crystals of TPAR1 (188 mg, 73.5%). ^{1}H NMR (300 MHz, $CDCl_3$): δ (ppm) 4.92 (2H, s, $-CH_2$COOH), 7.01 (2H, d, J = 8.79 Hz, aromatic), 7.14−7.19 (6H, m, aromatic), 7.31−7.37 (6H, m, aromatic), 7.71-(1H, s, −CH═). ESI-MS: m/z 445 ([M − H]$^-$). Anal. Calcd for $C_{24}H_{18}N_2O_3S_2$: C, 64.57; N, 6.27; H, 4.0. Found: C, 64.53; N, 6.18; H, 4.1.

TPAR2: A 300 mg (1.1 mmol) sample of **2** was dissolved in 5 mL of DMF and Vilsmeier reagent that was prepared from 5 mL of DMF and 0.6 mL of phosphorus oxychloride, and then the mixture was kept at 25 °C for Vilsmeier−Haack reaction of 3 h. After neutralization with 25% NaOH solution to pH 8, the product was extracted by column chromatography (hexane/ethyl acetate 10:1), resulting in 3-(4-(diphenylamino)phenyl)-acrylaldehyde (**3**) (276 mg, 83.2%). ^{1}H NMR (300 MHz, $CDCl_3$): δ (ppm) 6.54 (1H, dd, J = 8.0, 7.6 Hz, −CH═), 6.97 (2H, d, J = 8.4 Hz, aromatic), 7.10 (6H, q, J = 7.8 Hz, aromatic), 7.28(4H, t, J = 7.6 Hz, aromatic), 7.36 {3H, m, (2H, aromatic and 1H, −CH═)}, 9.61 (1H, d, J = 7.8 −CH═O). ESI-MS: m/z 300 ([M + H]$^+$).

The same procedure as for TPAR1 but with **3** (165 mg, 0.55 mmol) instead of **1** was used. TPAR2 was purified by column chromatography with use of silica gel and ethyl acetate−ethanol mixed solvent as the eluant (208 mg, 76.2%). ^{1}H NMR (300 MHz, DMSO-d_6): δ (ppm) 4.38 (2H, s, $-CH_2$COOH), 6.85−6.94 {3H, m, (2H, aromatic and 1H, −CH═)}, 7.08−7.17 (5H, m, aromatic), 7.28 (1H, d, J = 14.9 Hz, −CH═), 7.37(4H, t, J = 7.9 Hz, aromatic), 7.48 (1H, d, J = 11.4 Hz, −CH═), 7.57 (2H, d, J = 8.7 Hz, aromatic). ESI-MS: m/z 471 ([M − H]$^-$). Anal. Calcd for $C_{26}H_{20}N_2O_3S_2$: C, 66.10; N, 5.93; H, 4.24. Found: C, 66.05; N, 5.97; H, 4.33.

TPAR4: A procedure similar to that for TPAR1 but with **4** (165 mg, 0.55 mmol) instead of **1** was used. TPAR4 was purified by column chromatography, using silica gel and ethyl acetate−ethanol mixed solvent as the eluant (146 mg, 53.6%).

^{1}H NMR (300 MHz, DMSO-d_6): δ (ppm) 4.41 (2H, s, $-CH_2$-COOH), 5.23 (1H, d, J = 11.5 Hz, $-CH{=}CH_2$), 5.75 (1H, d, J = 16.8 Hz, $-CH{=}CH_2$), 6.71 (1H, dd, J = 10.9, 11.1 Hz, $-CH{=}$), 6.93 (2H, q, J = 8.9 Hz, aromatic), 7.08−7.24 (5H, m, aromatic), 7.37−7.52 (6H, m, aromatic), 7.66 (1H, s, $-CH{=}$). ESI-MS: m/z 471 ([M − H]$^-$). Anal. Calcd for $C_{26}H_{20}N_2O_3S_2$: C, 66.10; N, 5.93; H, 4.24. Found: C, 66.18; N, 5.87; H, 4.32.

TPAR5: A 655 mg (1.2 mmol) sample of **5** was dissolved in 10 mL of DMF and Vilsmeier reagent prepared from 5 mL of DMF and 0.6 mL of phosphorus oxychloride. The mixture was kept at 25 °C for Vilsmeier−Haack reaction of 3 h. After neutralization with 25% NaOH solution to pH 8, the product was extracted by column chromatography (petroleum ether/methylene chloride/ethyl acetate 7:3:1), resulting in 235 mg of 4-(*N*-phenyl-*N*-(4-vinylphenyl)amino)acrylaldehyde (**6**). ^{1}H NMR (300 MHz, DMSO-d_6): δ (ppm) 5.21 (1H, d, J = 11.7 Hz, $-CH{=}CH_2$), 5.74 (1H, d, J = 17.6 Hz, $-CH{=}CH_2$), 6.65−6.76 (2H, m, $-CH{=}$), 6.91 (2H, d, J = 8.7 Hz, aromatic), 7.05 (2H, d, J = 8.5 Hz, aromatic), 7.12−7.20 (3H, m, aromatic), 7.39 (2H, t, J = 7.5 Hz, aromatic), 7.45 (2H, d, J = 8.5 Hz, aromatic), 7.64 {3H, t, (2H, aromatic and 1H, $-CH{=}$)}, 9.59 (1H, d, J = 7.9 Hz, $-H{=}O$). ESI-MS: m/z 326 ([M + H]$^+$).

A procedure similar to that for TPAR1 but with **6** (179 mg, 0.55 mmol) instead of **1** was used. TPAR5 was purified by column chromatography, using silica gel and ethyl acetate−ethanol mixed solvent as the eluant (153 mg, 53.5%). ^{1}H NMR (300 MHz, DMSO-d_6): δ (ppm) 4.40 (2H, s, $-CH_2$COOH), 5.20 (1H, d, J = 11.7 Hz, $-CH{=}CH_2$), 5.73 (1H, d, J = 17.5 Hz, $-CH{=}CH_2$), 6.69 (1H, dd, J = 10.9, 11.1 Hz, $-CH{=}$), 6.84−6.95 {3H, m, (2H, aromatic and 1H, $-CH{=}$)}, 7.04 (4H, q, J = 8.7 Hz, aromatic), 7.16 (1H, t, J = 7.3 Hz, aromatic), 7.28−7.40 {4H, m, (3H, aromatic and 1H, $-CH{=}$)}, 7.43 (1H, d, J = 8.6 Hz, aromatic), 7.47 (1H, d, J = 11.5 Hz, $-CH{=}$), 7.57 (2H, d, J = 8.7 Hz, aromatic). ESI-MS: m/z 497 ([M − H]$^-$). Anal. Calcd for $C_{28}H_{22}N_2O_3S_2$: C, 67.46; N, 5.62; H, 4.42. Found: C, 67.41; N, 5.73; H, 4.36.

^{1}H NMR spectra were carried out by Varian Mercury V×300 at 300 MHz. The reported chemical shifts were against TMS. ESI-MS data were measured with LCQ AD (Thermofinnigan, USA). The elemental analysis was performed by Vanio-EL (Heraeus).

Photophysical and Electrochemical Measurements. Commercial TiO_2 (P25, Degussa AG, Germany, a mixture of ca. 30% rutile and 70% anatase) was used for the preparation of the nanocrystalline films. The TiO_2 paste consisting of 16.2% P25 and 4.5% ethyl cellulose in terpineol was first prepared, which was printed on a conducting glass (Nippon Sheet Glass, Hyogo, Japan, fluorine-doped SnO_2 over layer, sheet resistance of 10 Ω/sq) with a screen printing technique. The thickness of the TiO_2 film was controlled by selection of screen mesh size and repetition of printing. The film was dried in air at 120 °C for 30 min and calcined at 450 °C for 30 min under flowing oxygen before cooling to room temperature. The heated electrodes were impregnated with a 0.05 M titanium tetrachloride solution in a water-saturated desiccator at 70 °C for 30 min and then recalcined at 450 °C for 30 min.

The absorption spectra of the dyes either in solution or on the adsorbed TiO_2 films were measured by Jasco V-550. Fluorescence measurement was carried with a Cary Eclipse fluorescence spectrophotometer. Adsorption of the dye on the TiO_2 surface was done by soaking the TiO_2 electrode in a dry methanol solution of the dye (standard concentration 3×10^{-4} M) at room temperature for 24 h.

The Pt counter electrode (FTO conducting glass coated with a thin platinum layer) was prepared according to the literature.[4a] The morphologies of the as-prepared TiO_2 and Pt electrodes were investigated by scanning electron microscopy (SEM, JEOL JSM-6700F Field Emission).[19]

The oxidation potentials of the as-synthesized dyes adsorbed on the TiO_2 films were measured by differential pulse voltammetry (DPV), using a PARSTAT 2273 electrochemical analyzer.[20] In the case of DPV, the modulation time is 50 ms and the modulation amplitude is 25 mV with the step time of 100 ms, step potential of 5 mV, and step height of 2.0 mV. The three-electrode cell composed of a glassy carbon as the working electrode, a platinum wire as the counter electrode, and a $Ag/AgNO_3$ (in acetonitrile) as the reference electrode was calibrated by measuring the redox potential of ferrocene dissolved in acetonitrile/AcOH (7/1, v/v). The redox potential referenced to calibrated $Ag/AgNO_3$ was converted to the NHE (normal hydrogen electrode) reference scale. The glassy carbon electrode was polished with Al_2O_3 paste, cleaned thoroughly in an ultrasonic water bath, and washed with ethanol before each measurement. Dry acetonitrile/AcOH (7/1, v/v) containing 0.1 M tetrabutylammonium perchlorate was used as the supporting electrolyte. The solutions were purged with argon and stirred for 15 min before the measurements.

Solar cells were made by sealing the electrolyte (a mixture of 0.6 M DMPImI, 0.1 M LiI, 0.05 M I_2, acetonitrile as a solvent) between the photoanode (the dye-deposited TiO_2 film) and the counter electrode. The electrochemical impedance spectroscopy (EIS) was investigated by means of a PARSTAT 2273 electrochemical analyzer.

The photocurrent−voltage (I-V) characteristics of the solar cells were carried out using a Keithley 2400 digital source meter controlled by a computer. A 500 W xenon lamp served as the light source in combination with a band-pass filter (400−800 nm) to remove ultraviolet and infrared radiation to give 100 mW cm^{-2} at the surface of the test cell. Further calibration was carried out by a USB4000 plug-and-play miniature fiber optic spectrometer (Ocean company, USA) to gave an AM 1.5 simulated sunlight. The active electrode area was 0.16 cm^2.

The η of a DSC is calculated from the short current density (J_{sc}), the open voltage (V_{oc}), the fill factor of the cell (ff), and the intensity of the incident light (P_{in}) as follows[21]

$$\eta = \frac{J_{sc} V_{oc} \mathrm{ff}}{P_{in}}$$

A similar data acquisition system was used to control the IPCE measurement. Light from a 500 W xenon lamp was focused through a monochromator onto the photovoltaic cell under test. The IPCE values were determined between 400 and 800 nm. The IPCE was then calculated according to the following equation:

$$\mathrm{IPCE}(\lambda) = \frac{1240}{\lambda\ (\mathrm{nm})} \frac{J_{sc}\ (\mathrm{mA/cm^2})}{\phi\ (\mathrm{mw/cm^2})}$$

where λ is the wavelength and ϕ is the power of the incident radiation per unit area. Light intensities were measured with a USB4000 fiber optic spectrometer (Ocean company, USA). For comparison, the DSC performance with N3 dye was also measured at the same conditions.

Computational Methods. The Gaussian 03 package[22] was used for Density functional theory (DFT) calculations. To model the electronic state of TPAR2 adsorbed on the TiO_2 surface,

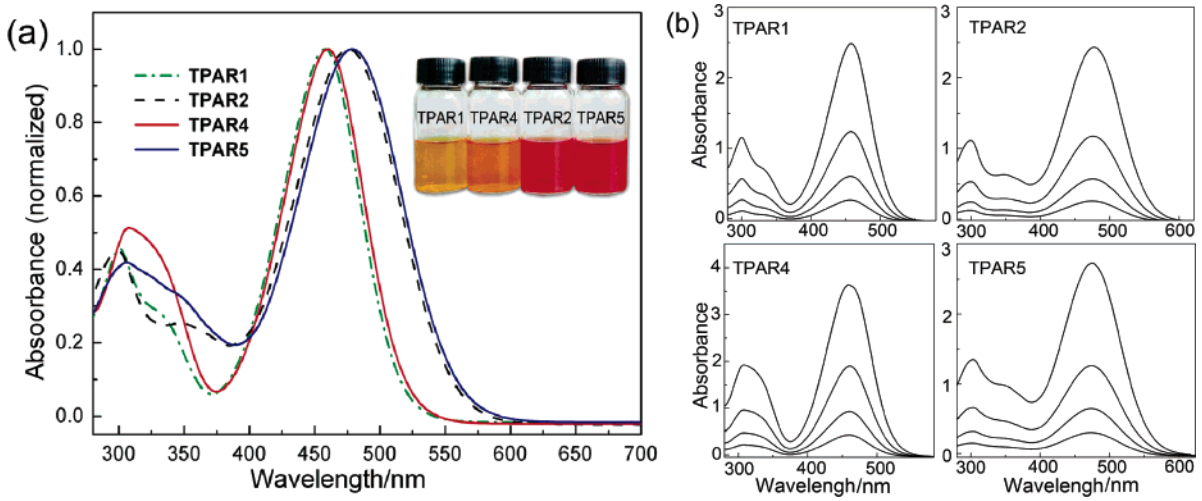

Figure 1. Absorption spectra of TPAR1, TPAR2, TPAR4, and TPAR5: (a) in methanol with normalized absorbance (inset photograph shows solutions of these dyes in glass bottles); (b) at different concentrations, 1×10^{-4}, 0.5×10^{-4}, 0.25×10^{-4}, and 0.125×10^{-4} M (from top to bottom).

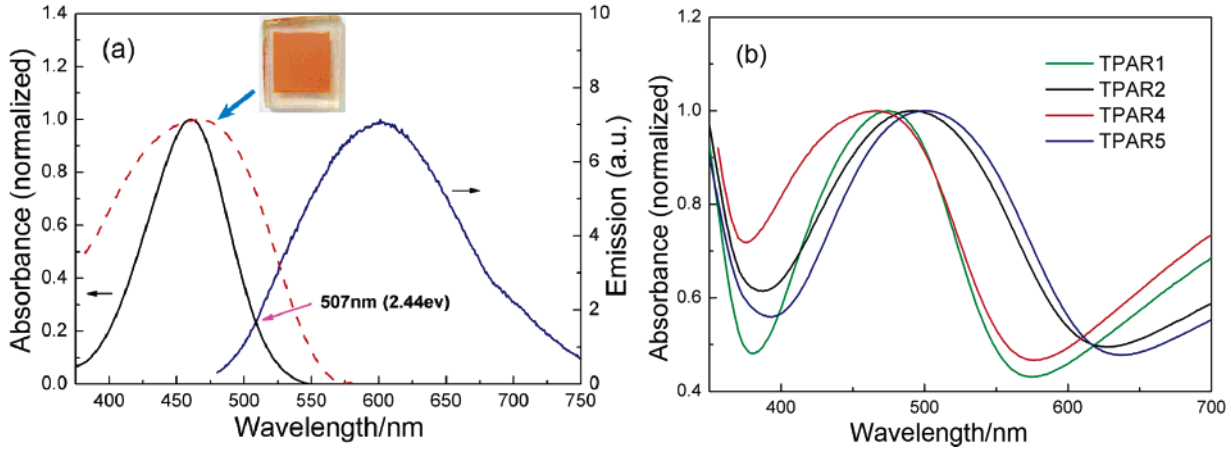

Figure 2. (a) Absorption (black solid line) and emission (blue solid line) spectra of TPAR4 in methanol as well as its absorption spectrum adsorbed on TiO_2 film (dash line, red) with normalized absorbance. The insert shows the photograph of the TiO_2 electrode coated with TPAR4. (b) Absorption spectra of the as-synthesized dyes adsorbed on TiO_2 films, which were measured in the diffuse reflectance mode.

we employed the dye's potassium salt because the dye must be bonded to the TiO_2 surface in its carboxylate form.[12a] We optimized the geometry of TPAR1 and TPAR4 using the B3LYP method with the 6-31+G(d) basis set. The stable geometry was confirmed by no imaginary frequency. Importantly, none of the frequency calculations generated negative frequencies, being consistent with an energy minimum for the optimized geometry.

Results and Discussion

UV−Vis Absorption/Emission Spectra. Figure 1a shows the absorption spectra of the four as-synthesized dyes in methanol, displaying two distinct absorption bands at around 300 and 470 nm, respectively. The weak absorption peaks at around 300 nm correspond to the $\pi-\pi^*$ electron transition; strong absorption peaks at around 470 nm can be assigned to an intramolecular charge transfer (ICT) between the TPA-based donor and the rhodanine-3-acetic acid,[23] which produce the efficient charge-separation excited state. It can be seen that the maximum absorption of TPAR2 and TPAR5 was obviously red-shifted in comparison with that of TPAR1 and TPAR4, which is due to the expansion of π-conjugation systems by introduction of the methine unit into the π-bridge. Compared to TPAR1, the spectrum of TPAR4 at short wave region is stronger and broader, which can be attributed to the modification of TPA by introduction of $CH_2{=}CH-$ to adjacent phenyl ring. A similar trend was observed from TPAR2 to TPAR5.

Figure 1b shows the spectra of the as-synthesized dyes at different concentrations: 1×10^{-4}, 0.5×10^{-4}, 0.25×10^{-4}, and 0.125×10^{-4} M. The λ_{max} and spectra shape were not changed, indicating that there is not any stacked aggregation[17a] in the solution state due to the prevention of the $\pi-\pi$ interactions between two adjacent parallel phenyl rings with the nonplanar structure of TPA.

Figure 2a shows the absorption and emission spectra of TPAR4 in methanol as well as the absorption spectrum of the dye adsorbed on TiO_2 film. The excitation wavelength for emission was 456 nm. The maximum absorption and emission in methanol are 461 and 602 nm, respectively. When the dye adsorbed on the TiO_2 surface, the absorption spectrum of TPAR4 was red-shifted from 461 nm to 467 nm, meaning that most of TPAR4 adsorbed on the TiO_2 surface in the monomeric state with only partially J-type aggregates.[12c] A slight red-shift and broadening of the absorption peak on the TiO_2 surface was also observed in other dyes (Figure 2b), which further confirms the formation of J-type aggregate. Although broadening of the absorption spectrum is desirable for light harvesting and improving the photocurrent, the J-type aggregates of dyes on

TABLE 1: Maximum Absorption and Emission Data of the As-Synthesized Dyes

dye	ϵ/M^{-1} cm^{-1} [a]	λ_{max}/nm[a]	λ_{max}/nm[b]	λ_{max}/nm[c]
TPAR1	23 700	458	540	475
TPAR2	22 800	476	565	491
TPAR4	36 400	461	602	467
TPAR5	25 600	474	640	501

[a] Absorption spectra of dyes measured in MeOH with the concentration of solution 5×10^{-5} M; ϵ is the extinction coefficient at λ_{max} of absorption. [b] Emission spectra of dyes measured in MeOH with the concentration of solution 5×10^{-5} M; ϵ is the extinction coefficient at λ_{max} of absorption. [c] Absorption spectra of dyes adsorbed on TiO_2.

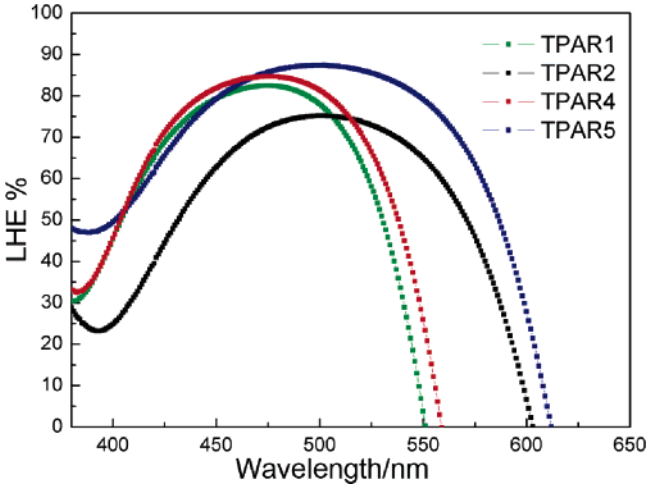

Figure 3. LHE spectra of the TiO_2 electrode coated with TPAR1, TPAR2, TPAR4, and TPAR5.

the TiO_2 surface should be avoided because molecular aggregations can largely decrease the electron injection yield. Thus, co-adsorption of dye molecules with chenodeoxycholic acid (DCA) on the TiO_2 film is necessary. The maximum absorption/emission and extinction coefficients of the as-synthesized dyes are summarized in Table 1. It is noted that among the four as-synthesized dyes, TPAR4 showed the highest extinction coefficients (ϵ) of 36 400 M^{-1} cm^{-1} at 461 nm, which is much higher than that of Ru-organic complex N3 (14 000 M^{-1} cm^{-1} in ethanol).[6] This result of extinction coefficients indicates that the as-synthesized metal-free organic dyes are beneficial to light harvesting.

The amounts of dye adsorbed on the TiO_2 films were estimated by desorbing the dye with basic solution. The surface concentrations were determined to be 0.84×10^{-7}, 0.48×10^{-7}, 0.78×10^{-7}, and 1.39×10^{-7} M cm^{-2} for TPAR1, TPAR2, TPAR4, and TPAR5, respectively. The light harvest efficiency (LHE) of the electrode was calculated by transmittance (T, %) and reflectance (R, %), using an integrating sphere (LHE(%) $= 100 - R - T$). The LHE spectra of the dye-coated electrodes are shown in Figure 3. The maximum LHE data are in the order of TPAR2 < TPAR1 < TPAR4 < TPAR5. Thus, efficient light-harvesting electrodes were obtained by the adsorption of the four as-synthesized dyes.

Electrochemical Properties. The oxidation potential of the triphenylamine dyes was determined from the peak potentials (E_p) by DPV (Figure 4). The oxidation potential vs NHE (E_{ox}) corresponds to the highest occupied molecular orbital (HOMO). The reduction potential vs NHE (E_{red}), which corresponds to the lowest unoccupied molecular orbital (LUMO), can be calculated from $E_{ox} - E_{0-0}$. Table 2 summarizes the electrochemical properties of the as-synthesized dyes. A negative shift of the E_{ox} (0.06 V) and a positive shift of the E_{red} (0.06 V) can

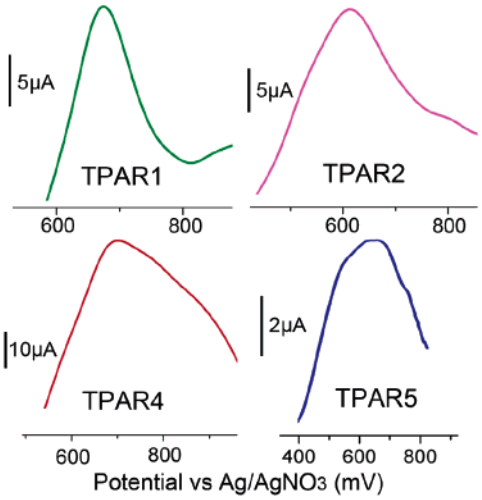

Figure 4. DPV of the triphenylamine-based dyes.

TABLE 2: Electrochemical Data of the As-Synthesized Dyes[a]

dye	λ_{int}/nm	E_{0-0}/eV	E_p/V	E_{ox}/V vs NHE	E_{red}/V vs NHE	E_{gap}/V
TPAR1	500	2.48	0.674	1.0	−1.48	0.98
TPAR2	526	2.36	0.613	0.94	−1.42	0.92
TPAR4	509	2.44	0.70	1.03	−1.41	0.91
TPAR5	547	2.27	0.645	0.97	−1.30	0.80

[a] E_{0-0} values were calculated from intersect of the normalized absorption and the emission spectra (λ_{int}): $E_{0-0} = 1240/\lambda_{int}$. The oxidation potential (E_{ox}) referenced to calibrated Ag/AgNO$_3$ was converted to the NHE reference scale: $E_{ox} = E_p + 0.325$ V, E_p is the peak potential of DPV. The reduction potential (vs NHE), E_{red}, was calculated from $E_{ox} - E_{0-0}$. E_{gap} is the energy gap between the E_{red} of dye and the CB level of TiO_2 (−0.5 V vs NHE).

be observed for TPAR2 vs TPAR1, which resulted in a decrease of the energy gap between the LUMO and HOMO. A similar condition was observed for TPAR5 vs TPAR4. This can be attributed to the expansion of the π-conjugation system by lengthening the methine chain. In the case of TPAR4 vs TPAR1 or TPAR5 vs TPAR2, a positive shift of the E_{ox} (0.03 V) and a positive shift of the E_{red} (0.07/0.09 V) was observed, which resulted from introduction of a $CH_2{=}CH-$ moiety into TPA.

As listed in Table 1, both the LUMO and HOMO levels of these dyes agreed with the requirement for an efficient sensitizer: First, their LUMO levels are negative of the CB level (−0.5 V vs NHE) of TiO_2, and the E_{gap} ranges from 0.80 to 0.98 eV. Assuming that energy gap of 0.2 eV is necessary for efficient electron injection,[12a] these driving forces are sufficiently large for effective electron injection. Second, HOMO levels of as-synthesized dyes were more positive than the iodine redox potential (0.4 V). Thus, these oxidized dyes can be regenerated from the reduced species in the electrolyte to give an efficient charge separation. Therefore, these dyes can be used as sensitizers which function well because the electron transfer in DSC is feasible.

Characterization of TiO_2 and Counter Electrode. Figure 5 shows the SEM images of the as-prepared TiO_2 film. The surface of the TiO_2 film is of porous character with nanoparticles (Figure 5a), which benefits the adsorption of dyes. The cross section analysis in Figure 5b illustrates that the film thickness is about 12 μm.

Figure 6a shows the photographs of the blank and the Pt mirror coated on FTO conducting glass. Figure 6b displays the SEM image of the Pt layer on the FTO conducting glass surface, indicating the homogeneous distribution of the Pt nanoparticles.

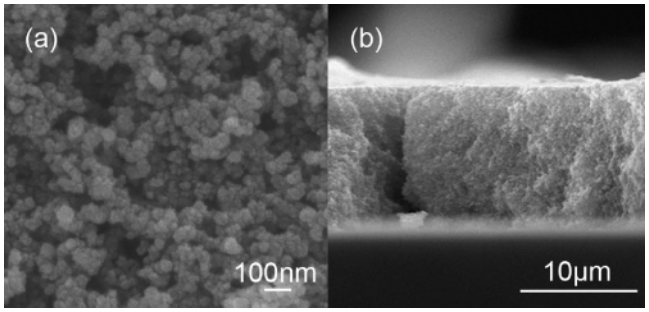

Figure 5. The SEM images of (a) the surface and (b) the cross section of the nanostructured TiO_2 thin film coated on the conducting glass.

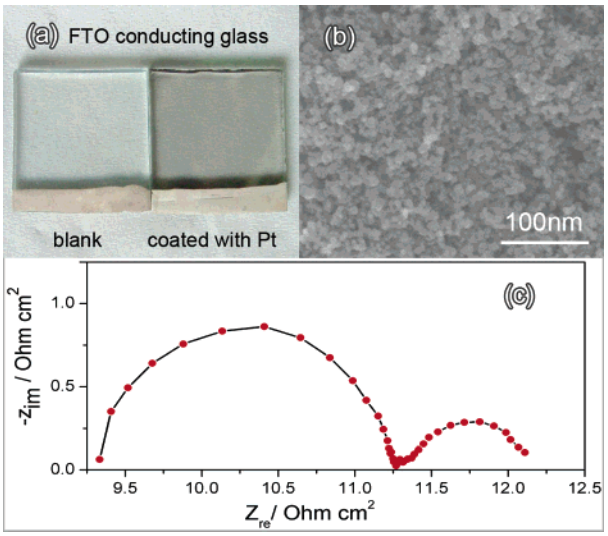

Figure 6. (a) Photographs of the blank and the Pt coated on FTO conducting glass. (b) The SEM image of Pt layer on the FTO conducting glass surface. (c) EIS for the DSC made of two Pt electrodes, which sandwiched the electrolyte.

To elucidate the catalytic activity of the Pt electrode, the electrical impedance spectrum (EIS) was further used to analyze the interfacial charge-transfer resistance (R_{CT}) between the electrolyte and the Pt electrode. The EIS was characterized with Zsimpwin software. Figure 6c shows the EIS of the sandwich-type cell made of two Pt electrodes. Two semicircles were observed in the measured frequency range of 10^6-10^{-2} Hz. The larger semicircle in the high-frequency region clearly reveals that the $2R_{CT}$ of the two Pt electrodes at the counter electrode/electrolyte interface is 1.78 Ω cm^2, meaning that the R_{CT} of one Pt electrode is 0.89 Ω cm^2. These data enable the efficient catalytic I_3^- reduction and electron transfer in DSC.

Solar Cell Performance. Figure 7 shows the IPCE of the as-prepared DSCs as a function of the wavelength. It can be seen that the photocurrent response of TPAR4 sensitized DCS is the best due to the IPCE exceeding 70% in the range of 440−500 nm. The maximum IPCE (81%) was obtained at 465 nm and this corresponds to almost unity quantum yield when light absorption and reflection by the conducting glass are taken into account. TPAR1 also shows a good photocurrent response with the maximum IPCE value of 72% at 470 nm. The decrease of the IPCE above 600 nm toward the long-wavelength region was ascribed to the decrease of light harvesting for both dyes. The IPCE of TPAR5 is much lower than that of TPAR1. In contrast, TPAR2 shows the lowest photocurrent response.

Figure 8 shows the $I-V$ curves of DSCs based on the as-synthesized dyes. The photovoltaic data were summarized in Table 3 in comparison with that of N3. Inconsistent with the result of IPCE, the photovoltaic data show the order of TPAR2 < TPAR5 < TPAR1 < TPAR4. For the most efficient sensitizer, TPAR4, an overall conversion efficiency of 5.84% was obtained with J_{sc} = 18.2 mA cm^{-2}, V_{oc} = 563 mV, and ff = 0.57. These values were comparable to those of the cell based on N3 (J_{sc} = 14.3 mA cm^{-2}, V_{oc} = 760 mV, ff = 0.62, and η = 6.70% with 0.5 M TBP contained electrolyte) measured in the same conditions. An increase in η of about 35% was obtained from TPAR1 to TPAR4, which can be ascribed to the improvement of the electron-donating ability. In contrast, the J_{sc} values of TPAR2 and TPAR5 were much lower than that of the other two dyes, leading to their less efficient photovoltaic performance.

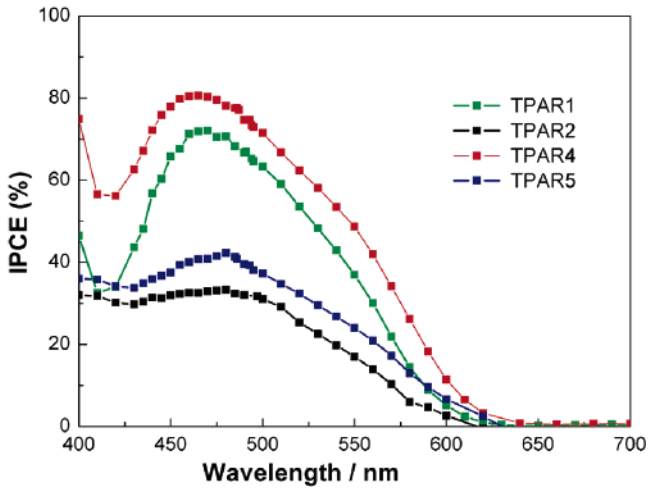

Figure 7. IPCE spectra for DSCs based on the as-synthesized dyes. The electrolyte was the mixture of 0.6 M DMPImI, 0.1 M LiI, and 0.05 M I_2 in acetonitrile.

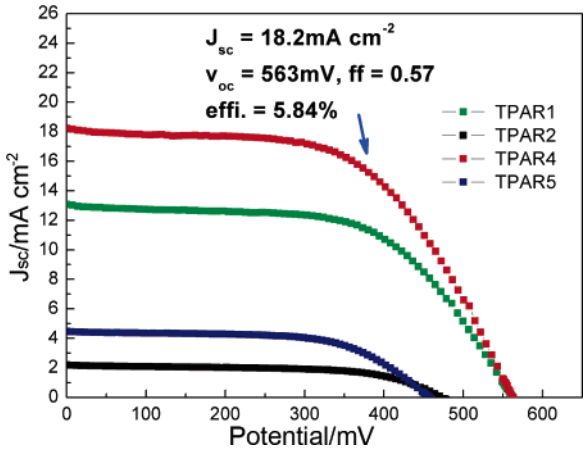

Figure 8. Current−potential ($I-V$) curves for the DSCs based on TPAR1, TPAR2, TPAR4, and TPAR5 under AM 1.5 irradiation (100 mW cm^{-2}). To prevent dye aggregations on the TiO_2 surface, 1 mM DCA was employed as a coadsorbate.

TABLE 3: Photovoltaic Performance of DSCs Sensitized with the As-Synthesized Dyes

dye	J_{sc}/mA cm^{-2}	V_{oc}/mV	ff	η/%
TPAR1	13.0	564	0.59	4.32
TPAR2	2.2	476	0.60	0.63
TPAR4	18.2	563	0.57	5.84
TPAR5	4.5	456	0.62	1.27
N3	14.3	760	0.62	6.70

Calculation Analysis of Dye Structure. Since TPAR1 and TPAR4 show better photovoltaic performance than that of TPAR2 and TPAR5, we further calculate their molecular structures with bidentate carboxylate coordination to potassium

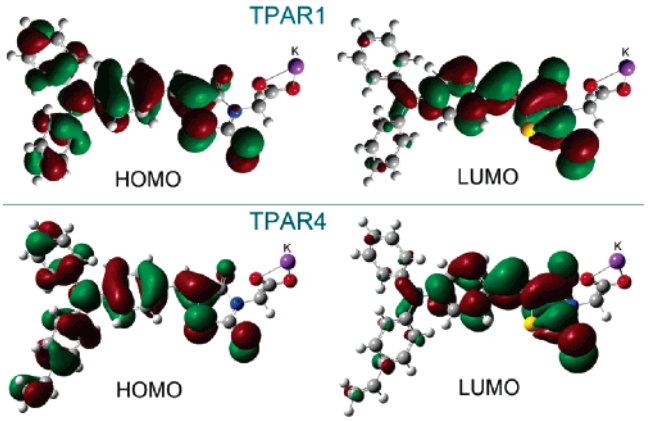

Figure 9. The frontier orbitals of the potassium salt of TPAR1 and TPAR4 optimized at the B3LYP/6-31+G(d) level.

(Figure 9). At the ground state (HOMO) for the two dyes, electrons are homogeneously distributed in both the electron donor group and the π bridge. However, at the excited state (LUMO) with light illumination, the intramolecular charge transfer occurs, leading to the electron movement from the donor group (left side) to the rhodanine ring (right side). Consequently, excited electrons are easily injected into TiO_2 via the acetic acid connected to the rhodanine ring.

As shown above, the photovoltaic performance of DSCs based on the as-synthesized dyes depends strongly on the molecular structure. The IPCE can be expressed by

$$\mathrm{IPCE}(\lambda) = \mathrm{LHE}(\lambda) \times \phi_{\mathrm{inj}} \times \eta_{\mathrm{coll}}$$

where LHE is the light harvesting efficiency, ϕ_{inj} is the quantum yield of electron injection, and η_{coll} is the electron collection efficiency, which depends on the structure and morphology of the TiO_2 layer.[24] Since the LHE spectra and the η_{coll} of TPAR4- and TPAR1-coated electrodes are almost the same, the main factor affecting the IPCE is the ϕ_{inj}. The only structural difference between TPAR4 and TPAR1 is the electron donor unit. Obviously, a stronger donor unit is able to generate more electrons under the same light excitation, which benefits the electron injection. It is probably that ϕ_{inj} of a DSC based on TPAR4 is higher than that of TPAR1, thus leading to an increase of IPCE. Better IPCE values are reflected in their J_{sc} value that is mainly responsible for energy conversion efficiency.

As a comparison, TPAR2 and TPAR5 showed better light harvesting ability (absorption spectra and LHE). However, they exhibited lower IPCE than that of TPAR1 and TPAR4. This may be due to their serious self-quenching of the electronically excited state, which results from the occurrence of cis−trans isomerization and the disorder alignment of chromophores in *J*-like aggregates, thereby decreasing the ϕ_{inj} greatly.[9c] Many other organic dyes also suffered from the long π-bridge. For example, Mc[2,1] (benzothiazole merocyanine dye) exhibits a low IPCE value.[9d] In the case of TPAR2, its lower LHE due to a small amount of dye adsorbed is another reason for the low IPCE compared to TPAR5.

Conclusions

We developed four triphenylamine-based metal-free organic dyes (TPAR1, TPAR2, TPAR4, and TPAR5), which have shown great potential as light sensitizers in DCSs. This type of dye has a simple structure and exhibits good photovoltaic performance. Introduction of a CH_2=CH− group into the electron-donor unit increased the electron density of the donor moiety that largely resulted in improved photovoltaic performance. The expansion of the π-conjugated system was achieved by increasing the length of the methine unit, which decreased IPCE. It is noted that TPAR4-sensitized DSC showed the best η of 5.84% with a remarkable J_{sc} of 18.2 mA cm^{-2} under AM 1.5 irradiation (100 mW cm^{-2}). This indicated that efficient electron injection from the excited dyes to the conduction band of TiO_2 occurred. It is evident that increasing the electron density of donor moiety is a very effective way to improve the performance of dye. Attempts to further improve the η of triphenylamine dye-sensitized DSC will concentrate on molecular design based on TPAR4 dye. And to better understand the title compounds, the dynamics of electron transport and recombination, as well as the stability of DSCs based on the as-synthesized dyes, will be studied in detail in our next work.

Acknowledgment. This work was supported by the National NSFC (20325102 and 50631020) and 973 Program (2005CB623607). The DFT calculations were supported by Virtual Laboratory for Computational Chemistry of CNIC and Supercomputing Center of CNIC, Chinese Academy of Sciences.

Supporting Information Available: ^{1}H NMR spectra and the effect of 4-*tert*-butylpyridine (TBP) on the DSCs performance with the as-synthesized dyes. This material is available free of charge via the Internet at http://pubs.acs.org.

References and Notes

(1) (a) O'Regan, B.; Grätzel, M. *Nature* **1991**, *353*, 737. (b) Grätzel, M. *Nature* **2001**, *414*, 338.

(2) (a) Wang, P.; Zakeeruddin, S. M.; Comte, P.; Exnar, I.; Grätzel, M. *J. Am. Chem. Soc.* **2003**, *125*, 1166. (b) Kubo, W.; Kambe, S.; Nakade, S.; Kitamura, T.; Hanabusa, K.; Wada, Y.; Yanagida, S. *J. Phys. Chem. B* **2003**, *107*, 4374. (c) Kumar, R.; Sharma, A. K.; Parmar, V. S.; Watterson, A. C.; Chittibabu, K. G.; Kumar, J.; Samuelson L. A. *Chem. Mater.* **2004**, *16*, 4841.

(3) (a) Law, M.; Greene, L. E.; Johnson, J. C.; Saykally, R.; Yang, P. *Nat. Mater.* **2005**, *4*, 455. (b) Adachi, M.; Murata, Y.; Takao, J.; Jiu, J.; Sakamoto, M.; Wang, F. *J. Am. Chem. Soc.* **2004**, *126*, 14943. (c) Zhang, D. S.; Downing, J. A.; Knorr, F. J.; McHale, J. L. *J. Phys. Chem. B* **2006**, *110*, 21890.

(4) (a) Papageorgiou, N.; Maier, W. F.; Grätzel, M. *J. Electrochem. Soc.* **1997**, *144*, 876. (b) Cai, F. S.; Chen, J.; Xu, R. S. *Chem. Lett.* **2006**, *35*, 1266.

(5) (a) Gregg, B. A. *Coord. Chem. Rev.* **2004**, *248*, 1215. (b) Frank, A. J.; Kopidakis, N.; Lagemaat, J. *Coord. Chem. Rev.* **2004**, *248*, 1165. (c) O'Regan, B. C.; Bakker, K.; Kroeze, J.; Smit, H.; Sommeling, P.; Durrant, J. R. *J. Phys. Chem. B.* **2006**, *110*, 17155. (d) Hoertz, P. G.; Mallouk, T. E. *Inorg. Chem.* **2005**, *44*, 6828.

(6) Nazeeruddin, M. K.; Kay, A.; Rodicio, I.; Humphry-Baker, R.; Müller, E.; Liska, P.; Vlachopoulos, N.; Grätzel, M. *J. Am. Chem. Soc.* **1993**, *115*, 6382.

(7) Nazeeruddin, M. K.; Péchy, P.; Renouard, T.; Zakeeruddin, S. M.; Humphry-Baker, R.; Comte, P.; Liska, P.; Cevey, L.; Costa, E.; Shklover, V.; Spiccia, L.; Deacon, G. B.; Bignozzi, C. A.; Grätzel, M. *J. Am. Chem. Soc.* **2001**, *123*, 1613.

(8) Grätzel, M. *Inorg. Chem.* **2005**, *44*, 6841.

(9) (a) Khazraji, A. C.; Hotchandani, S.; Das, S.; Kamat, P. V. *J. Phys. Chem. B.* **1999**, *103*, 4693. (b) Sayama, K.; Hara, K.; Mori, N.; Satsuki, M.; Suga, S.; Sukagoshi, S.; Abe, Y.; Sugihara, H.; Arakawa, H. *Chem. Commun.* **2000**, 1173. (c) Sayama, K.; Tsukagoshi, S.; Mori, T.; Hara, K.; Ohga, Y.; Shinpou, A.; Abe, Y.; Suga, S.; Arakawa, H. *Sol. Energy Mater. Sol. Cells* **2003**, *80*, 47. (d) Sayama, K.; Tsukagoshi, S.; Hara, K.; Ohga, Y.; Shinpou, A.; Abe, Y.; Suga, S.; Arakawa, H. *J. Phys. Chem. B* **2002**, *106*, 1363.

(10) (a) Wang, Z. S.; Li, F. Y.; Huang, C. H.; Wang, L.; Wei, M.; Jin, L. P.; Li, N. Q. *J. Phys. Chem. B* **2000**, *104*, 9676. (b) Wang, Z. S.; Li, F. Y.; Huang, C. H. *Chem. Commun.* **2000**, 2063. (c) Wang, Z. S.; Li, F. Y.; Huang, C. H. *J. Phys. Chem. B* **2001**, *105*, 9210. (d) Chen, Y. S.; Li, C.; Zeng, Z. H.; Wang, W. B.; Wang, X. S.; Zhang, B. W. *J. Mater. Chem.* **2005**, *15*, 1654.

(11) (a) Takechi, K.; Sudeep, P. K.; Kamat, P. V. *J. Phys. Chem. B* **2006**, *110*, 16169. (b) Cherepy, N. J.; Smestad, G. P.; Grätzel, M.; Zhang, J. Z. *J. Phys. Chem. B* **1997**, *101*, 9342. (c) Zhao, W.; Hou, Y. J.; Wang,

X. S.; Zhang, B. W.; Cao, Y.; Yang, R.; Wang, W. B.; Xiao, X. R. *Sol. Energy Mater. Sol. Cells* **1999**, *58*, 173. (d) Ehret, A.; Stuhl, L.; Spitler, M. T. *Electrochim. Acta* **2000**, *45*, 4553. (e) Ehret, A.; Stuhl, L.; Spitler, M. T. *J. Phys. Chem. B* **2001**, *105*, 9960−9965. (f) Chen, X. Y.; Guo, J. H.; Peng, X. J.; Guo, M.; Xu, Y. Q.; Shi, L.; Liang, C. L.; Wang, L.; Gao, Y. L.; Sun, S. G.; Cai, S. M. *J. Photochem. Photobiol. A* **2005**, *171*, 231.

(12) (a) Hara, K.; Sato, T.; Katoh, R.; Furube, A.; Ohga, Y.; Shinpo, A.; Suga, S.; Sayama, K.; Sugihara, H.; Arakawa, H. *J. Phys. Chem. B* **2003**, *107*, 597. (b) Hara, K.; Kurashige, M.; Dan-oh, Y.; Kasada, C.; Shinpo, A.; Suga, S.; Sayama, K.; Arakawa, H. *New J. Chem.* **2003**, *27*, 783. (c) Wang, Z. S.; Hara, K.; Dan-oh, Y.; Kasada, C.; Shinpo, A.; Suga, S.; Arakawa, H.; Sugihara, H. *J. Phys. Chem. B* **2005**, *109*, 3907.

(13) (a) Ferrere, S.; Zaban, A.; Gregg, B. A. *J. Phys. Chem. B* **1997**, *101*, 4490. (b) Ferrere, S.; Gregg, B. A. *New J. Chem.* **2002**, *26*, 1155.

(14) (a) Horiuchi, T.; Miura, H.; Uchid, S. *Chem. Commun.* **2003**, 3036. (b) Ito, S.; Zakeeruddin, S. M.; Humphry-Baker, R.; Liska, P.; Charvet, R.; Comte, P.; Nazeeruddin, M. K.; Péchy, P.; Takata, M.; Miura, H.; Uchida, S.; Grätzel, M. *Adv. Mater.* **2006**, *18*, 1202.

(15) (a) Koumura, N.; Wang, Z.-S.; Mori, S.; Miyashita, M.; Suzuki, E.; Hara, K. *J. Am. Chem. Soc.* **2006**, *128*, 14256. (b) Tan, S.; Zhai, J.; Fang, H.; Jiu, T.; Ge, J.; Li, Y.; Jiang, L.; Zhu, D. *Chem. Eur. J.* **2005**, *11*, 6272.

(16) (a) Hara, K.; Sato, T.; Katoh, R.; Furube, A.; Yoshihara, T.; Murai, M.; Kurashige, M.; Ito, S.; Shinpo, A.; Suga, S.; Arakawa, H. *Adv. Funct. Mater.* **2005**, *15*, 246. (b) Li, S. L.; Jiang, K. J.; Shao, K. F.; Yang, L. M. *Chem. Commun.* **2006**, 2792.

(17) (a) Kitamura, T.; Ikeda, M.; Shigaki, K.; Inoue, T.; Anderson, N. A.; Ai, X.; Lian, T. Q.; Yanagida, S. *Chem. Mater.* **2004**, *16*, 1806. (b) Velusamy, M.; Thomas, K. R. J.; Lin, J. T.; Hsu, Y.; Ho, K. *Org. Lett.* **2005**, *7*, 1899. (c) Hagberg, D. P.; Edvinsson, T.; Marinado, T.; Boschloo, G.; Hagfeldt. A.; Sun, L. *Chem. Commun.* **2006**, 2245.

(18) Behl, M.; Hattemer, E.; Brehmer, M.; Zentel, R. *Macromol. Chem. Phys.* **2002**, *203*, 503.

(19) Gou, X. L.; Cheng, F. Y.; Shi, Y. H.; Zhang, L.; Peng, S. J.; Chen, J.; Shen, P. W. *J. Am. Chem. Soc.* **2006**, *128*, 7222.

(20) Li, W. Y.; Li, C. S.; Zhou, C. Y.; Ma, H.; Chen, J. *Angew. Chem., Int. Ed.* **2006**, *45*, 6009.

(21) Hagfeldt, A.; Grätzel, M. *Acc. Chem. Res.* **2000**, *33*, 269.

(22) Frisch, M. J.; Trucks, G. W.; Schlegel, H. B.; Scuseria, G. E.; Robb, M. A.; Cheeseman, J. R.; Montgomery, J. A., Jr.; Vreven, T.; Kudin, K. N.; Burant, J. C.; Millam, J. M.; Iyengar, S. S.; Tomasi, J.; Barone, V.; Mennucci, B.; Cossi, M.; Scalmani, G.; Rega, N.; Petersson, G. A.; Nakatsuji, H.; Hada, M.; Ehara, M.; Toyota, K.; Fukuda, R.; Hasegawa, J.; Ishida, M.; Nakajima, T.; Honda, Y.; Kitao, O.; Nakai, H.; Klene, M.; Li, X.; Knox, J. E.; Hratchian, H. P.; Cross, J. B.; Bakken, V.; Adamo, C.; Jaramillo, J.; Gomperts, R.; Stratmann, R. E.; Yazyev, O.; Austin, A. J.; Cammi, R.; Pomelli, C.; Ochterski, J. W.; Ayala, P. Y.; Morokuma, K.; Voth, G. A.; Salvador, P.; Dannenberg, J. J.; Zakrzewski, V. G.; Dapprich, S.; Daniels, A. D.; Strain, M. C.; Farkas, O.; Malick, D. K.; Rabuck, A. D.; Raghavachari, K.; Foresman, J. B.; Ortiz, J. V.; Cui, Q.; Baboul, A. G.; Clifford, S.; Cioslowski, J.; Stefanov, B. B.; Liu, G.; Liashenko, A.; Piskorz, P.; Komaromi, I.; Martin, R. L.; Fox, D. J.; Keith, T.; Al-Laham, M. A.; Peng, C. Y.; Nanayakkara, A.; Challacombe, M.; Gill, P. M. W.; Johnson, B.; Chen, W.; Wong, M. W.; Gonzalez, C.; Pople, J. A.; *Gaussian 03*, Revision C.02; Gaussian, Inc.: Wallingford, CT, 2004.

(23) Roquet, S.; Cravino, A.; Leriche, P.; Alévêque, O.; Frère, P.; Roncali, J. *J. Am. Chem. Soc.* **2006**, *128*, 3459.

(24) Kalyanasundaram, K.; Grätzel, M. *Coord. Chem. Rev.* **1998**, *77*, 347.